Journal of Nuclear Medicine, published on August 11, 2016 as doi:10.2967/jnumed.116.176206

First-in-Human Imaging with ^{89}Zr-Df-IAB2M Anti-PSMA Minibody in Patients with Metastatic Prostate Cancer: Pharmacokinetics, Biodistribution, Dosimetry, and Lesion Uptake

Neeta Pandit-Taskar[1,2], Joseph A. O'Donoghue[3], Shutian Ruan[1], Serge K. Lyashchenko[4], Jorge A. Carrasquillo[1,2], Glenn Heller[5], Danny F. Martinez[6], Sarah M. Cheal[7], Jason S. Lewis[1,2,4,7], Martin Fleisher[8], Jennifer S. Keppler[9], Robert E. Reiter[9], Anna M. Wu[9], Wolfgang A. Weber[1,2], Howard I. Scher[6,10], Steven M. Larson[1,2,7], Michael J. Morris[6,10]

Affiliation/department:
[1] Radiology, Memorial Sloan Kettering Cancer Center (MSK), New York, NY
[2] Radiology, Weill Cornell Medical College (WCMC), New York, NY
[3] Medical Physics, MSK
[4] Radiochemistry & Molecular Imaging Probes Core, MSK
[5] Epidemiology & Biostatistics, MSK
[6] Medicine, MSK
[7] Molecular Pharmacology Program, MSK
[8] Laboratory Medicine, MSK
[9] ImaginAb, Inc., Inglewood, CA
[10] Medicine, WCMC

Corresponding author:
Neeta Pandit-Taskar, MD
1275 York Avenue, Box 77
New York, NY 10065
pandit-n@mskcc.org

Research Support: ImaginAb, Inc.; DOD Clinical Consortium (#PC071610); MSK's Radiochemistry & Molecular Imaging Probe Core and Biostatistics Core (CCSG P30 CA008748).

Word count: 4,997

Running foot: ^{89}Zr-IAB2M minibody prostate Ca imaging

ABSTRACT

We conducted a Phase I dose escalation study with ^{89}Zr-desferrioxamine-IAB2M (^{89}Zr-IAB2M), an anti-PSMA minibody, in patients with metastatic prostate cancer (mPC). **Methods**: Patients received 185 MBq (5 mCi) of ^{89}Zr-IAB2M and Df-IAB2M at total mass doses of 10 mg (n=6), 20 mg (n=6), and 50 mg (n=6). Whole-body (WB) and serum clearance, normal organ and lesion uptake, and radiation-absorbed dose were estimated and the effect of mass escalation was analyzed. **Results**: Eighteen patients were injected and scanned without side effects. WB clearance was monoexponential with median biological half ($T_{1/2}$b) of 215 h, while serum clearance showed biexponential kinetics with a median $T_{1/2}$b of 3.7 h (12.3 %/L) and 33.8 h (17.9 %/L). The RAD estimates were 1.67, 1.36, and 0.32 mGy/MBq to liver, kidney, and marrow, respectively, with an effective dose of 0.41 mSv/MBq (1.5 rem/mCi). Both skeletal and nodal lesions were detected with ^{89}Zr-IAB2M, most visualized by 48 h imaging. **Conclusion**: ^{89}Zr-IAB2M is safe and demonstrates favorable biodistribution and kinetics for targeting mPC. Imaging with 10 mg minibody mass provides optimal biodistribution, and imaging at 48 h post-injection provides good lesion visualization. Assessment of lesion targeting is being studied in detail in an expansion cohort.

Key Words: ^{89}Zr- IAB2M, minibody, PSMA, prostate cancer imaging, dosimetry.

INTRODUCTION

Currently, conventional imaging for metastatic prostate cancer (mPC) cannot reliably assess viable disease. We have previously shown the feasibility of using radiolabeled anti-prostate-specific membrane antigen (PSMA) antibodies to target prostate cancer (*1,2,3*). However, the optimal lesion detection is seen 6-8 days post-injection (p.i.) due to slower blood clearance of the full antibody. Smaller molecules and antibody fragments such as minibody and diabody have faster clearance, and reach higher tumor-to-background ratios earlier (*4,5*). Fragments below 60 kDa are filtered through the glomerular system, leading to significant kidney excretion (*6-10*)—less ideal for prostate cancer imaging. IAB2M is an 80 kDa minibody genetically engineered from the parent antibody J591 that targets the extracellular domain of PSMA (Fig. 1). The lack of Fc receptor interaction domains on the minibody makes it pharmacologically inert to Fc-mediated effector functions (*7-9*).

Preclinical studies demonstrated faster clearance and rapid biodistribution with efficient target penetration, allowing for high-contrast images within a few hours p.i. (*11-13*). In mice, ^{89}Zr-IAB2M (*14*) showed properties similar to ^{89}Zr-huJ591antibody but with significantly faster blood clearance and high uptake at 24 h p.i. in PSMA-positive tissue (*15*).

In view of the preclinical data, ^{89}Zr-IAB2M may facilitate earlier lesion detection in patients, compared to its full parent antibody. As an initial component

of analytic validation for biomarkers for advanced prostate cancer (*16*), we performed this first-in-human evaluation of ^{89}Zr-IAB2M imaging in patients with mPC.

MATERIALS AND METHODS

This is a prospective Phase I/IIa, open-label, non-randomized, single-dose imaging study with ^{89}Zr-IAB2M performed under an Investigational New Drug application (IND #118810). The protocol was Institutional Review Board-approved and all patients provided written informed consent (trial registration ID: NCT01923727).

Patients

Patient eligibility required histologically confirmed prostate cancer and progressive disease by imaging, defined as new lesion(s) on Tc99m-methylene diphosphonate bone scan (MDP) or increase in size or new sites of soft tissue disease on CT or MRI or by biochemical criteria.

The aims were to evaluate the safety and feasibility of ^{89}Zr-IAB2M in mPC; assess pharmacokinetics, biodistribution, and radiation dosimetry; and determine optimal mass dose and imaging time for lesion detection.

All patients had baseline imaging including MDP, CT, and/or MRI and FDG-PET scans performed as standard of care within four weeks of ^{89}Zr-IAB2M

administration. The total IAB2M mass dose was escalated from 10 to 20 to 50 mg in three cohorts of six patients each. All patients underwent multiple serial imaging, WB count measurements, and blood sampling (Fig. 2).

^{89}Zr-IAB2M Minibody Formulation and Injection

IAB2MTwas supplied by Catalent Pharma Solutions (Somerset, NJ). Desferrioxamine was obtained from Macrocyclics (Dallas, TX) and conjugated to IAB2M under Good Manufacturing Practice guidelines at Isotherapeutics Group (Angleton, TX) and supplied in vials to MSK for radiolabeling (*17*). ^{89}Zr radionuclide production and radiolabeling of Df-IAB2M was performed using previously described methods (*14,18*). ^{89}Zr was labeled to 2-3 mg of Df-IAB2M. The radiolabeling efficiency was >80%; radiochemical purity was >95%, as determined by instant thin layer chromatography; and immunoreactivity was >90%, as determined by Lindmo cell binding assay (*19*).

^{89}Zr-IAB2M Administration

The radiolabeled minibody was administered IV over 5-10 minutes in combination with cold Df-IAB2M to make up the designated total mass balance for the specific cohort. No premedications were administered. Patients were monitored for at least one hour p.i. for any reactions or adverse events; side effects and reactions were graded per CTC 4.0 criteria.

Blood samples were evaluated at baseline and approximately one month p.i. for human anti-human antibody (HAHA), performed at Intertek (San Diego, CA) using a GLP-validated electrochemiluminescent assay.

PET Imaging

Each patient underwent four WB PET/CT scans including vertex to mid-thigh; lower extremities were included in those with known lesions by conventional imaging. Emission scans were acquired on a GE Discovery STE scanner in 3D mode for three minutes per field of view (FOV) on the day of injection; 24 h p.i., 48-72 h p.i. (five min/FOV), and 96-120 h (7 min/FOV). PET/CT scans were performed with a low-dose CT for attenuation correction (single scan with 80 mA current and three with 10 mA current). Images were reconstructed using OSEM parameters (2 iterations; 16 subsets) and attenuation correction.

Whole-body counts were also obtained using a probe with NaI (Tl) scintillation detector at a fixed geometry (3 m from probe to patient). Measurements were taken after ^{89}Zr-IAB2M infusion, first prior to voiding p.i., immediately after first voiding, and at each later imaging time-point (five total). Background-corrected geometric mean values were used for clearance curve fitting.

Serum Clearance Measurements

Multiple blood samples were measured for activity concentration to obtain percent injected activity/liter (% IA/L). Samples included a baseline sample prior to ^{89}Zr-Df-IAB2M infusion, followed by 5, 15, 30, 60, and 120-240 min p.i., and subsequently at the time of each PET scan, totaling 7-8 samples.

Derivation of Whole-Body and Serum Kinetic Parameters

WB activity data and serum activity data was fitted using the SAAM II software application (*20*). Values of cumulated activity per unit administered activity (residence time) for WB (in h) and serum (in h/L), τ, were calculated according to the formula $\tau = \tilde{A} / A_0$, where Ã, the cumulated activity, was estimated by integrating the activity-time curve and administered activity (A_0). Effective and biological clearance rates and corresponding half-times were derived from the fitted curves.

Uptake in Normal Organs and Lesions

Regions of interest (ROI) were drawn on images within normal organs and target lesions using dedicated software (Hermes Medical Solutions, Chicago, IL). A subset of index lesions (maximum of 5 per patient) was analyzed for uptake trends using mean standard uptake value (SUV) adjusted to lean body mass (SUV_{LBM}) for organs and maximum SUV for lesions (*21*). Activity concentration-

time area under the curve (AUC) correlates were estimated by trapezoidal integration. Whole-organ AUC was estimated by multiplying the activity concentration AUC by organ mass.

Baseline values of organ mass representing standard mean were taken from the OLINDA/EXM software application (*22*); rescaling was performed if the actual patient mass differed by more than 15% from the standard value (73.7 kg), per prior method (*23*). Residence times were derived by dividing the whole-organ AUC by the administered activity. Corresponding values for heart contents and red marrow were derived from serum (*24*). Residence times for the remainder of body were derived by subtracting all individually estimated residence times from the WB residence time. Absorbed radiation doses to the whole body and various organs were calculated using the OLINDA/EXM software application (*22*).

RESULTS

A total of 18 patients with mPC were studied (Supplemental Table 1). Injection was tolerated well, with no reactions seen in any patients. The mean injected activity was 188.7±2.96 MBq (5.1±0.8 mCi) and mean mass of radiolabeled minibody was 1.86±0.35 mg.

HAHA analysis showed immunoreactivity to Df-IAB2M in 3/16 evaluable samples. The titers ranged from 25 to 625 and did not correlate with total protein dose, nor were they associated with any side effects that differentiated them from

patients who did not generate HAHA. A repeat serum IgG analysis in these patients showed no significant increase in IgG subclasses 1-4.

Whole-Body and Serum Kinetics

The WB clearance conformed to monoexponential function (Fig. 3). The median WB biological half-lifes ($T_{1/2}b$) for 10, 20, and 50 mg were 142.9 h (range 118.7-256.7 h), 222.0 h (range 165.0-364.8 h), and 235.8 h (range 210.7-450.1 h), respectively (Table 1). WB clearance was slower at higher mass (50 mg) than the lower masses (10 and 20 mg). Effective half-lifes for WB clearance ($p=0.04$) for 10 vs. 20 mg and 10 vs. 50 mg ($p=0.01$) were significantly different, while no significant difference was seen between 20 vs. 50 mg ($p=0.54$).

Serum clearance was biexponential, characterized by an initial rapid phase followed by a slow phase. The average effective half-times were 4.8±2.5 h (range 1.2-8.9 h) for the fast component and 23.8±4.6 h (range 17.4-32.3 h) for the slow component (Fig. 3A, Table 1). The mean AUC was 1038±290 %ID h/L, Cmax was 31.2±6.3 %ID/L, and Vd was 3.3±0.7 L.

A tendency toward slower serum clearance was apparent at higher minibody mass; significant differences were noted for both 20 and 50 mg minibody doses compared to the lowest mass dose (10 mg) (Fig. 3, Table 1). The inter-group differences also reflect the modification of the data collection scheme partway through cohort II (20 mg) to include a later time-point. While no

significant difference between early- or late-phase effective or biological clearance was observed between 10 vs. 20 mg doses, significant differences were seen for the late-phase effective as well as biological clearance for both 10 and 20 vs. 50 mg minibody level ($p=0.01$).

Biodistribution

Prominent activity was seen in the blood pool, which decreased with time (Fig. 4A). Increased liver and GI tract activity was seen over time, and renal activity increased with plateau beyond 48 h. No significant activity was seen in the bladder and no significant urinary clearance was noted; the WB counts before and after first void showed an average post-void value of 98.6±3.1% of the pre-void activity. Gall bladder activity was seen in some patients and was more prominent in earlier images up to 24 h, thereafter decreasing with time. Activity seen in the GI tract was more prominent in later images, suggesting possible hepatobiliary clearance (range 1-10%; median value of 5%). Mild diffuse uptake was seen in the spleen, decreasing over time. Minimal activity was seen in bone in delayed imaging, with no significant uptake in the lung. The distribution appeared similar for all IAB2M mass doses on PET/CT imaging (Fig. 4).

Normal Organ Uptake

Liver uptake was characterized by a gradual increase over time, but did

not plateau (Fig. 5A). Maximum SUV_{LBM} at 48 h p.i. ranged between 4.5-5.5 (mean 5.3±0.7) rising to 5.5-7.0 (mean 6.1±1.0) at 120 h p.i. in patients for whom later imaging was performed. Renal uptake also increased with time and plateaued at 48 h p.i. (maximum SUV_{LBM} range of 6-8; mean 6.5±1.3).

A reduction in liver uptake was noted at the highest mass dose, while no definite relationship between mass dose and renal uptake was apparent. Uptake in spleen was highest in initial imaging (~2 h p.i.) and diminished thereafter, likely relating to blood pool activity. Typical SUV_{LBM} for spleen was approximately 3 at 48 h p.i. and later. Uptake in normal bone was low, with SUV_{LBM} values in the range of 0.3-1.5.

Radiation Doses to Normal Organs

The average absorbed radiation dose estimates are summarized in Table 2. A mass-based rescaling was used in 10/18 patients and the maximum effective mass was invoked in 3/10 cases. No significant differences were noted in normal organ RAD among the three ^{89}Zr-IAB2M mass dose groups. The highest organ dose was observed for the liver (1.67±0.30 mGy/MBq), followed by kidney (1.36±0.26 mGy/MBq).

Lesion Targeting in Patients

^{89}Zr-IAB2M antibody scans were positive in a total of 17/18 patients (Figs. 4, 6) with bone lesions targeted in 9/18 patients and soft tissue disease seen in 14/18 patients. In comparison, bone scan (MDP) and FDG was positive in 9/18 and 6/18 patients for bone lesions, respectively, while for nodal/soft tissue disease, CT and FDG scans were positive in 14/18 and 10/18 patients, respectively. In two patients, a single site of disease per patient was identified only by ^{89}Zr-IAB2M scan. ^{89}Zr-IAB2M imaging detected a total of 147 bone and 82 soft tissue or nodal lesions. Pathology correlation in 12 lesions showed concordance of scan and pathology findings in 11 patients.

Uptake of ^{89}Zr-IAB2M in Lesions

SUV trend was examined in 25 bone and 39 soft tissue lesions. Lesions were seen as early as 24 hours p.i. with increased lesion number and SUV seen at 48 h (Fig. 4) and 72-120 h; generally, highest uptake was seen at the last imaging time-point (Figs. 4B, 5B). Higher uptake is seen in bone lesions (SUV_{MAX} 13.8±8.6; range 2.5-42) compared to soft tissue (SUV_{MAX} 7.0±3.5; range 2.7-14.7). The SUV_{MAX} for bone lesions at 48 h was 29.6, 19.5, and 8.7 for 10, 20, and 50 mg, respectively, while for soft tissue or nodal lesions it was 14.7, 14.8, and 7.7, respectively. The SUX_{MAX} tumor/normal background (T/B) ratios ranged from 1.9-45.8 at 48 h and 1.4-97.6 at 72-120 h for bone lesions, and 1.0-30.2 at 48 h and 1.3-35.6 at 72-120 h for soft tissue (Supplemental Fig. 1).

Highest uptake was seen in the 10 mg cohort, mostly related to high bone uptake compared to the 20 and 50 mg cohorts; however, it was significant for 10 vs. 50 mg only (p=0.04). Uptake was slightly higher in soft tissue lesions at 20 mg compared to 10 mg; however, this is limited by the smaller number of lesions (n=8). Generally, uptake was lower in both bone and soft tissue lesions at 50 mg compared to 10 or 20 mg (p=0.04 and 0.02, respectively). The T/B ratio for lesions in different antibody mass cohorts at 48 h ranged from 3.8-26.2 in cohort I, 1.9-45.9 for cohort II, and 4.6-6.0 for cohort III for bone lesions (all inter-cohort comparisons were significant), while for soft tissue it ranged between 2.4-12.6, 5.2-28.7, and 1.0-11.2, respectively, for cohorts I, II, and III. These were non-significant for 10 vs. 20 mg (p=0.09) but significant for 10 vs. 50 mg and 20 vs. 50 mg (p=0.03 and 0.02, respectively).

While lesions were detectable as early as 24 h p.i. with ^{89}Zr-IAB2M imaging, more lesions were detectable at later time-points at 48 h in all cohorts. Delayed imaging at 72-120 h p.i. was performed in 9 patients (3 patients at 20 mg and 6 patients at 50 mg minibody mass) that showed an additional 7 lesions in 3 patients (1 bone lesion in the 20 mg cohort and 6 nodes in the 50 mg cohort) at 120 h imaging. Of these, a single additional bone lesion was seen in a rib that was negative on other concurrent imaging. Other additional detected lesions included: 5 nodes in cervical or axillary region with SUV range of 1.9-5.6 that were subcentimeter in size (0.3-0.5 cm) and negative by CT and FDG with no disease

noted on follow-up studies. An additional subcentimeter (0.7 cm) inguinal node (SUV 4.8) seen in another patient remained stable in follow-up studies; other inguinal nodes were also noted in this patient, and the most prominent one was biopsied and found to be negative on pathology.

Pathology correlation obtained for 5 bone and 7 soft tissue lesions showed 4/4 true-positive bone lesions and one true-negative bone lesion for ^{89}Zr-IAB2M; correlation for soft tissue lesions showed 6/7 true-positive lesions for ^{89}Zr-IAB2M. 10/10 pathology positive lesions for metastatic disease were positive on ^{89}Zr-IAB2M.

DISCUSSION

Despite the availability of multiple imaging modalities and advances in imaging techniques, accurate assessment of metastatic disease in prostate cancer remains limited with standard imaging, emphasizing the need for novel and improved molecular imaging methods that allow direct visualization of tumor. Radiolabeled choline PET imaging has been shown to target disease (*25*); however, this is not routinely available in the US. Recently, small-molecule targeting agents directed against PSMA have been evaluated, allowing earlier imaging (*2,3, 26,27*). As an ongoing programmatic effort to develop biomarkers for prostate cancer (*28*), we continue to explore novel imaging and therefore undertook this Phase I imaging study with the small antibody fragment IAB2M.

^{89}Zr-IAB2M is easy to administer and well tolerated with no observed infusion-related side effects. A higher titer for HAHA was detected in three patients. Assuming that an increase in IgG2 would indicate a possible HAHA interference with the assay for serum IgG detection, thereby suggesting functionality and clinical significance, no significant increase in IgG subclasses was noted in any patients (*29*).

The biodistribution of ^{89}Zr-IAB2M was broadly similar to that of the parent full-size antibody ^{89}Zr-huJ591 (*3*). The mechanism of liver accumulation is likely multifactorial, including reactivity with PSMA, minibody metabolism, and retention of metabolized radiometal. Tracer accumulation in kidney was again primarily in the renal cortex, probably due to known PSMA expression in the tubules, with no activity in the pelvicalyceal system or urine as expected based on size—an advantage over smaller molecules, making it more desirable for prostate cancer imaging by eliminating interference from urinary activity in the ureters and bladder. No significant salivary gland or lacrimal gland uptake was seen, unlike small-molecule PSMA ligands (*30*).

As expected, serum clearance was faster for ^{89}Zr-IAB2M minibody than ^{89}Zr-huJ591 (Fig. 7A), allowing for earlier lesion detection within 24-48 h vs. 6-8 days with ^{89}Zr-huJ591 (Fig. 7B). Organ radiation doses were broadly similar between ^{89}Zr-IAB2M and ^{89}Zr-huJ591 (Supplemental Fig. 2); the liver received the highest radiation dose with minibody, similar to the full antibody, but uptake

was overall slightly less with the minibody (1.67 mGy/MBq for ^{89}Zr-IAB2M vs. 2.08 for ^{89}Zr-huJ591).

The findings suggest that 10 mg mass of ^{89}Zr-IAB2M allows for optimal biodistribution for imaging. The minibody mass escalation resulted in slower WB and serum clearance with higher masses—an observation consistent with previous antibody studies (*1,31,32*). No significant difference in biodistribution between 10 mg and 20 mg minibody dose was noted. While a suggestion of decreased liver uptake at the 50 mg minibody dose was observed, the difference was small and nonsignificant ($p=0.10$ for 10 vs. 50 mg). No consistent pattern was seen between renal uptake and IAB2M mass, suggesting that the mild uptake seen is probably related to receptor-based uptake in renal tubules, with no significant effect of minibody mass on the uptake.

Lesion targeting was seen at all IAB2M mass doses. Lesion uptake (SUV) between 10 and 20 mg minibody dose was not significantly different. While higher uptake values were seen in lesions at the 10-20 mg levels than the 50 mg minibody dose (Supplemental Fig. 1), this finding is limited by variations in the disease extent and bone vs. soft tissue extent of metastatic disease in patients within each cohort, and is hence not conclusive. The initial 10 and 20 mg patient cohorts had a greater preponderance of bone lesions while most patients in the 50 mg cohort had predominantly soft tissue lesions, which may contribute to the apparent differences in lesion uptake and the observed mass effects, thereby

limiting the comparison among the cohorts. Further assessment is ongoing in an expansion cohort to assess any possible differences between 10 vs. 20 mg for lesion uptake and detection. However, the initial analysis suggests that 10 mg minibody is adequate for imaging.

This data supports the ability of ^{89}Zr-IAB2M minibody imaging to detect lesions earlier than full antibodies (*28*). Based on the initial results of visual assessment of lesion detection and lesion uptake patterns (Supplemental Fig. 1), imaging at 48 h p.i. provides good visualization of both bone and soft tissue lesions. In this preliminary analysis, no significant incremental lesion detection was noted for osseous sites beyond 48 h p.i. A single additional bone site noted on the delayed imaging was not confirmed by other imaging. While more nodal sites were detected at 120 h p.i., these were likely not related to true disease, based on stability or resolution noted on follow-up clinical and imaging data. While this must be confirmed in a larger group of patients, it is possible that non-specific uptake in benign/inflammatory sites may occur that may be more prominently seen in delayed imaging.

In our study, we injected patients with ~5 mCi of ^{89}Zr-Df-IAB2M minibody for imaging. Image patients with lower activity of ^{89}Zr is possible, as has been previously reported (*33*). Additionally, due to high contrast and relatively earlier imaging of lesions by 48 h p.i., we anticipate that adequate lesion detection may be achieved with lower levels of ^{89}Zr than used in this study. A

detailed analysis of lesion targeting in a larger patient cohort and assessment of imaging with lower injected activity dosing is underway.

CONCLUSION

PET imaging with ^{89}Zr-Df-IAB2M is feasible, well tolerated, shows favorable biodistribution in patients with advanced prostate cancer, and targets both bone and soft tissue lesions. Imaging with 10 mg minibody mass provides optimal biodistribution, and imaging at 48 h p.i. provides good visualization of lesions. Further analysis of lesion detection is ongoing in an expanded study.

ACKNOWLEDGMENTS

Funding sources: ImaginAb, Inc.; DOD Clinical Consortium (#PC071610); MSK's Radiochemistry & Molecular Imaging Probe Core and Biostatistics Core (CCSG P30 CA008748).

REFERENCES

1. Pandit-Taskar N, O'Donoghue JA, Morris MJ, et al. Antibody mass escalation study in patients with castration-resistant prostate cancer using (111)In-J591: lesion detectability and dosimetric projections for (90)Y radioimmunotherapy. *J Nucl Med.* 2008;49:1066–1074.

2. Morris MJ, Divgi CR, Pandit-Taskar N, et al. Pilot trial of unlabeled and indium-111-labeled anti-prostate-specific membrane antigen antibody J591 for castrate metastatic prostate cancer. *Clin Cancer Res.* 2005;11:7454–7461.

3. Pandit-Taskar N, O'Donoghue JA, Beylergil V, et al. ^{89}Zr-huJ591 immuno-PET imaging in patients with advanced metastatic prostate cancer. *Eur J Nucl Med Mol Imaging.* 2014;41:2093–2105.

4. Knowles SM, Wu AM. Advances in immuno-positron emission tomography: antibodies for molecular imaging in oncology. *J Clin Oncol.* 2012;30:3884–3892.

5. Olafsen T, Sirk SJ, Olma S, Shen CK, Wu AM. ImmunoPET using engineered antibody fragments: fluorine-18 labeled diabodies for same-day imaging. *Tumour Biol.* 2012;33:669–677.

6. Wong JY, Chu DZ, Williams LE, et al. Pilot trial evaluating an ^{123}I-labeled 80-kilodalton engineered anticarcinoembryonic antigen antibody fragment (cT84.66 minibody) in patients with colorectal cancer. *Clin Cancer Res.* 2004;10:5014–5021.

7. Wu AM, Olafsen T. Antibodies for molecular imaging of cancer. *Cancer J.* 2008;14:191–197.

8. Wu AM. Engineered antibodies for molecular imaging of cancer. *Methods.* 2014;65:139–147.

9. Wu AM. Antibodies and antimatter: the resurgence of immuno-PET. *J Nucl Med.* 2009;50:2–5.

10. Freise AC, Wu AM. In vivo imaging with antibodies and engineered fragments. *Mol Immunol.* 2015;67:142–152.

11. Wu AM, Senter PD. Arming antibodies: prospects and challenges for immunoconjugates. *Nature Biotech.* 2005;23:1137–1146.

12. Leyton JV, Olafsen T, Lepin EJ, et al. Humanized radioiodinated minibody for imaging of prostate stem cell antigen-expressing tumors. *Clin Cancer Res.* 2008;14:7488–7496.

13. Olafsen T, Betting D, Kenanova VE, et al. Recombinant anti-CD20 antibody fragments for small-animal PET imaging of B-cell lymphomas. *J Nucl Med.* 2009;50:1500–1508.

14. Holland JP, Divilov V, Bander NH, Smith-Jones PM, Larson SM, Lewis JS. Zr-89-DFO-J591 for immunoPET of prostate-specific membrane

antigen expression in vivo. *J Nucl Med.* 2010;51:1293–1300.
15. Viola-Villegas NT, Sevak KK, Carlin SD, et al. Noninvasive imaging of PSMA in prostate tumors with (89)Zr-labeled huJ591 engineered antibody fragments: the faster alternatives. *Mol Pharm.* 2014;11:3965–3973.
16. U.S. Department of Health and Human Services FDA Center for Drug Evaluation and Research (CDER). Guidance for Industry and FDA Staff Qualification Process for Drug Development Tools. Jan 2014; accessed at http://www.fda.gov/downloads/drugs/guidancecomplianceregulatoryinformation/gui, dances/ucm230597.pdf.
17. Vosjan MJ, Perk LR, Visser GW, et al. Conjugation and radiolabeling of monoclonal antibodies with zirconium-89 for PET imaging using the bifunctional chelate p-isothiocyanatobenzyl-desferrioxamine. *Nature Protocols.* 2010;5:739–743.
18. Holland JP, Sheh Y, Lewis JS. Standardized methods for the production of high specific-activity zirconium-89. *Nucl Med Biol.* 2009;36:729–739.
19. Lindmo T, Boven E, Cuttitta F, Fedorko J, Bunn PA, Jr. Determination of the immunoreactive fraction of radiolabeled monoclonal antibodies by linear extrapolation to binding at infinite antigen excess. *J Immunol Methods.* 1984;72:77–89.
20. Barrett PH, Bell BM, Cobelli C, et al. SAAM II: simulation, analysis, and modeling software for tracer and pharmacokinetic studies. *Metabolism.* 1998;47:484–492.
21. Morgan DJ, Bray KM. Lean body mass as a predictor of drug dosage. Implications for drug therapy. *Clin Pharmacokinet.* 1994;26:292–307.
22. Stabin MG, Sparks RB, Crowe E. OLINDA/EXM: the second-generation personal computer software for internal dose assessment in nuclear medicine. *J Nucl Med.* 2005;46:1023–1027.
23. Wahl RL, Kroll S, Zasadny KR. Patient-specific whole-body dosimetry: principles and a simplified method for clinical implementation. *J Nucl Med.* 1998;39:14S-20S.
24. Sgouros G, Stabin M, Erdi Y, et al. Red marrow dosimetry for radiolabeled antibodies that bind to marrow, bone, or blood components. *Med Physics.* 2000;27:2150–2164.
25. Bauman G, Belhocine T, Kovacs M, Ward A, Beheshti M, Rachinsky I. 18F-fluorocholine for prostate cancer imaging: a systematic review of the literature. *Prostate Cancer Prostatic Dis*. 2012;15:45–55.
26. Bander NH, Nanus DM, Milowsky MI, Kostakoglu L, Vallabahajosula S, Goldsmith SJ. Targeted systemic therapy of prostate cancer with a monoclonal antibody to prostate-specific membrane antigen. *Sem Oncol.* 2003;30:667–677.
27. Bander NH, Milowsky MI, Nanus DM, Kostakoglu L, Vallabhajosula S,

Goldsmith SJ. Phase I trial of (177)lutetium-labeled J591, a monoclonal antibody to prostate-specific membrane antigen, in patients with androgen-independent prostate cancer. *J Clin Oncol.* 2005;23:4591–4601.

28. Pandit-Taskar N, O'Donoghue JA, Beylergil V, et al. (89)Zr-huJ591 immuno-PET imaging in patients with advanced metastatic prostate cancer. *Eur J Nucl Med Mol Imaging.* 2014;41:2093–2105.

29. Schauer U, Stemberg F, Rieger CH, et al. IgG subclass concentrations in certified reference material 470 and reference values for children and adults determined with the binding site reagents. *Clin Chem.* 2003;49:1924–1929.

30. Afshar-Oromieh A, Malcher A, Eder M, et al. PET imaging with a [68Ga]gallium-labelled PSMA ligand for the diagnosis of prostate cancer: biodistribution in humans and first evaluation of tumour lesions. *Eur J Nucl Med Mol Imaging.* 2013;40:486–495.

31. Morris MJ, Divgi C, Kelly WK, et al. Phase I trial to evaluate J591 as a vascular targeting agent in patients with advanced solid tumors. *P Am Assoc Canc Res Ann Meeting.* 2003;44:803–803.

32. Morris MJ, Divgi CR, Pandit-Taskar N, et al. Pilot trial of unlabeled and indium-111-labeled anti-prostate-specific membrane antigen antibody J591 for castrate metastatic prostate cancer. *Clin Cancer Res.* 2005;11:7454–7461.

33. Boerjesson PKE, Jauw YWS, de Bree R, et al. Radiation dosimetry of Zr-89-labeled chimeric monoclonal antibody U36 as used for immuno-PET in head and neck cancer patients. *J Nucl Med.* 2009;50:1828–1836.

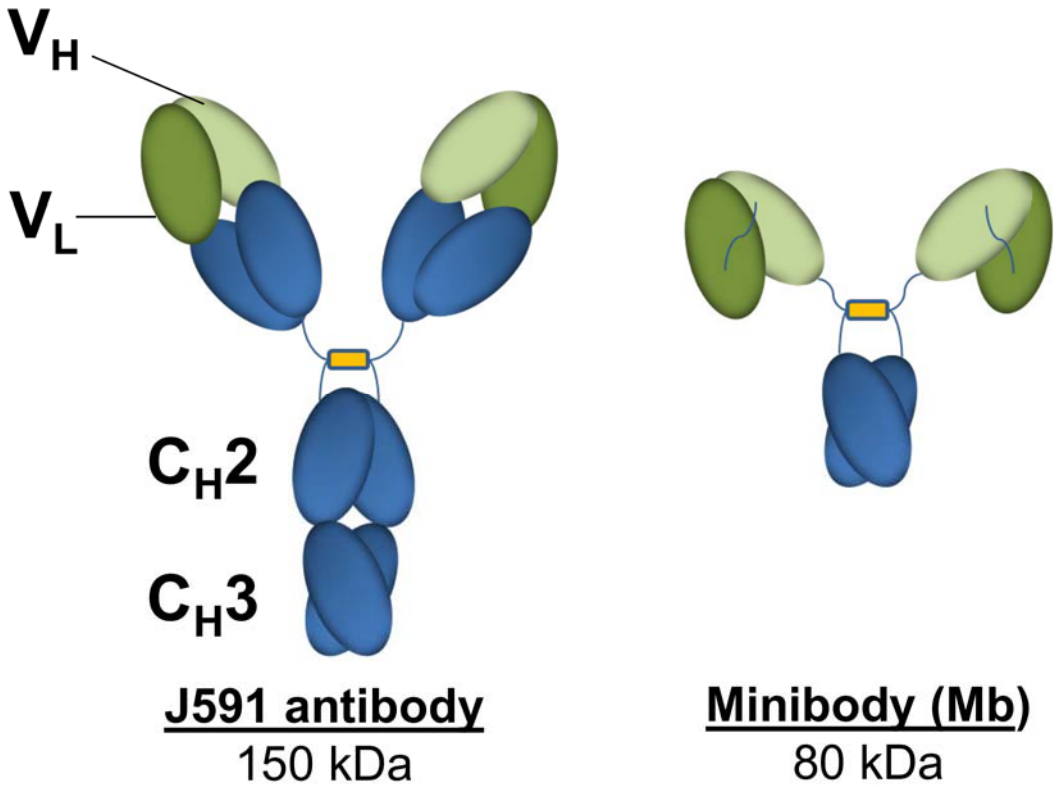

FIGURE 1. Structure of intact antibody and IAB2M

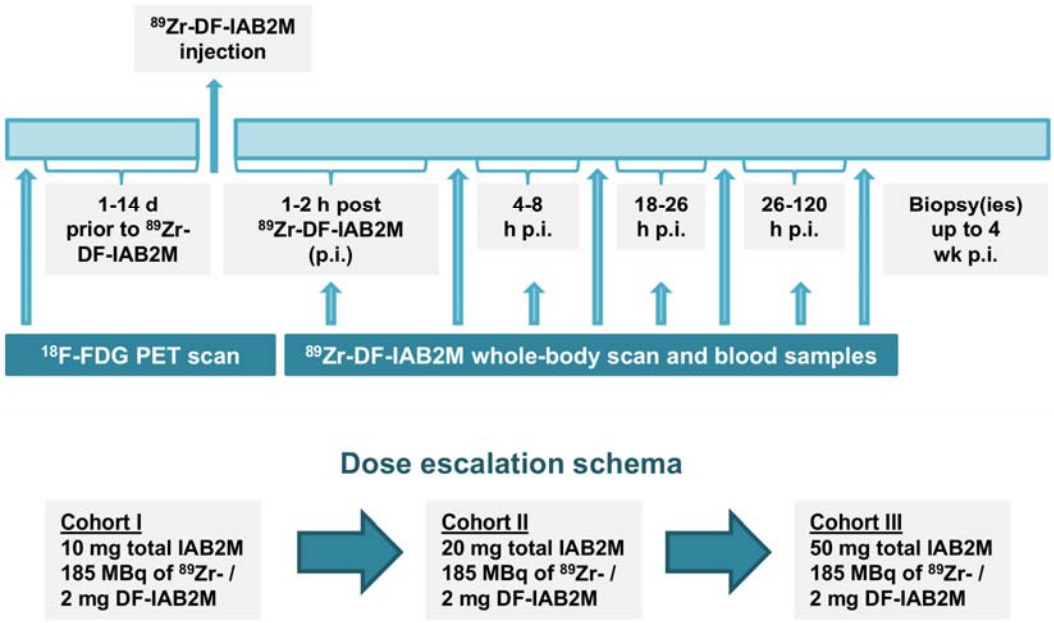

FIGURE 2. Study schema

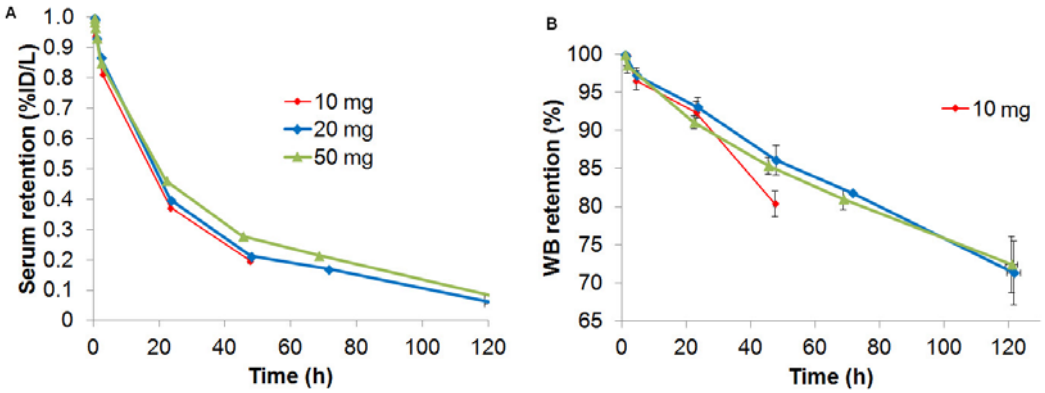

FIGURE 3. Serum (A) and whole-body clearance (B) of ^{89}Zr-IAB2M shown in aggregate mean values of biologic (i.e., decay-corrected) activity retention.

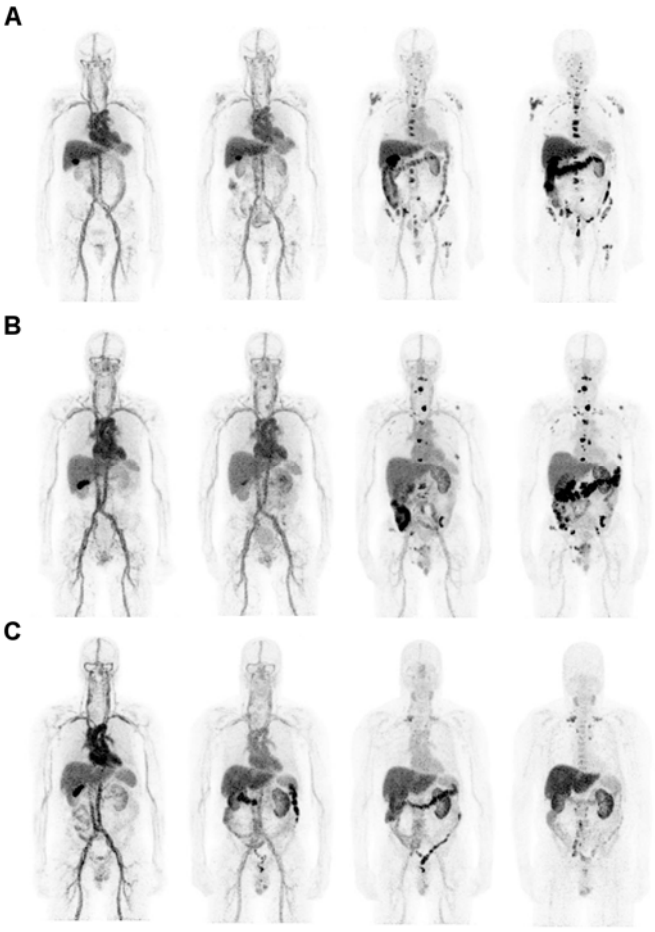

FIGURE 4. Biodistribution of ^{89}Zr-IAB2M in a patient: 10 mg IAB2M mass (A); 20 mg IAB2M mass (B); and 50 mg IAB2M mass (C).

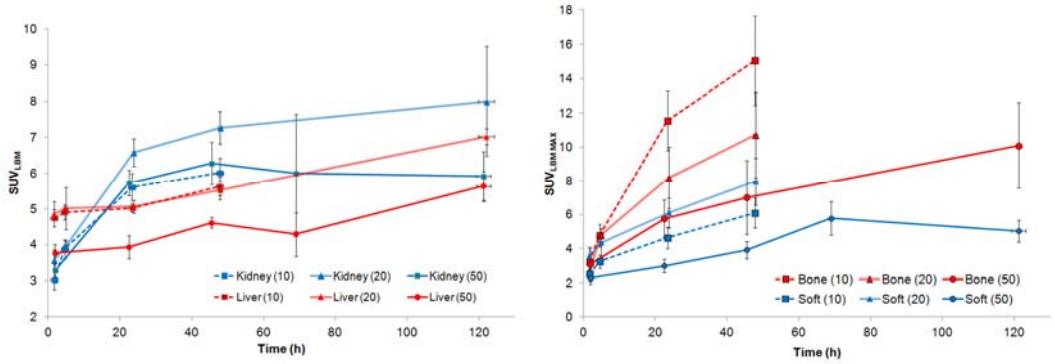

FIGURE 5. Normal organ uptake (A); lesion uptake (B).

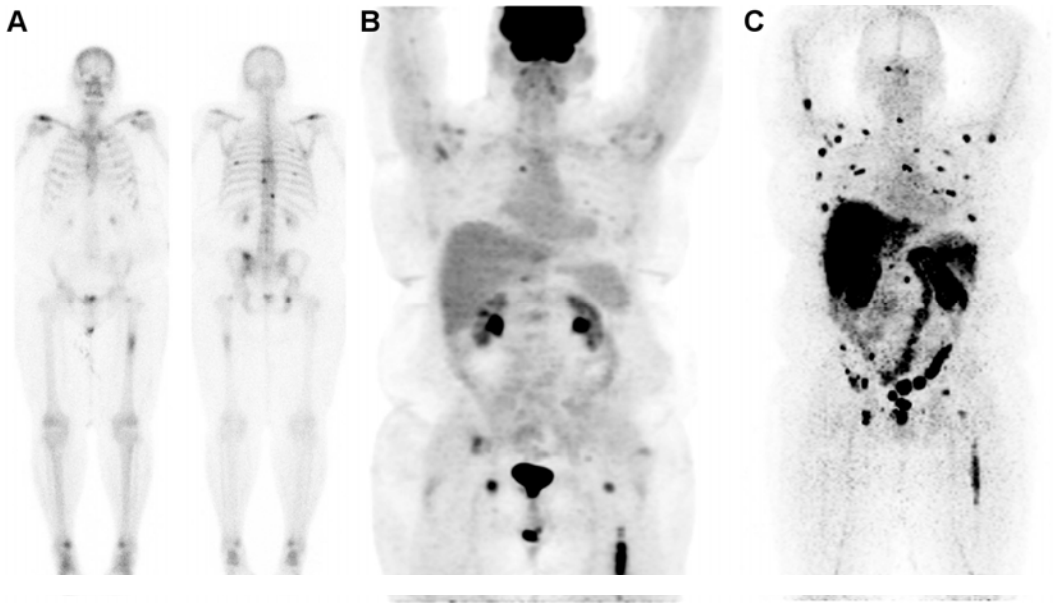

FIGURE 6. Lesion targeting with ^{89}Zr-IAB2M in mPC patient. 99mTc-MDP bone scan (A) shows lesions in vertebrae and ribs. FDG-PET scan (B) shows uptake in left femur and faint uptake in vertebral lesions. ^{89}Zr-IAB2M imaging (C) shows more images compared to bone scan or FDG (arrows).

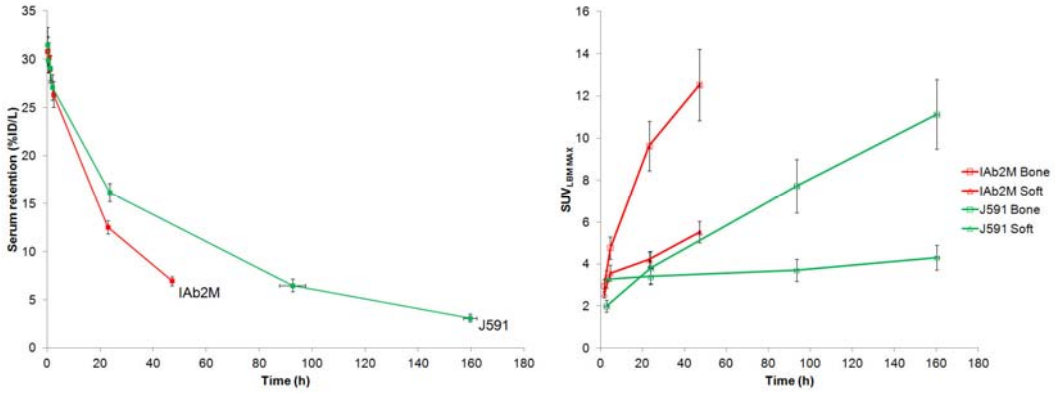

FIGURE 7. ^{89}Zr-IAB2M vs. ^{89}Zr-J591: serum clearance (A); lesion uptake (B).

TABLE 1. Whole-body and serum kinetic parameters as median (range).

Whole-Body and Serum Kinetic Parameters				
Parameter	**10 mg**	**20 mg**	**50 mg**	**Overall Mean**
WB T1/2 biol(h)	143(119-257)	222(165-365)	236(211-450)	225±82
WB T1/2 eff(h)	51(47-60)	58(53-65)	59(57-67)	57±5
Serum A1 (%/L)	8(5-14)	12(6-23)	13(9-16)	12±5
Serum T1/2 α eff(h)	3.1(1.2-5.7)	5.0(1.9-8.0)	6.3(2.2-8.9)	5±3
Serum A2 (%/L)	18(15-27)	18(14-29)	18(13-27)	19±5
Serum T1/2 β eff(h)	19(17-27)	22(19-27)	28(25-32)	24±5

Table 2. Absorbed radiation dose estimates (mGy/MBq) of ^{89}Zr-IAb2M to organs

	All patients		Cohort I	Cohort II	Cohort III
Target Organ	**Mean(SD)**	**Min-Max**	**Mean(SD)**	**Mean(SD)**	**Mean(SD)**
Adrenals	0.53(0.06)	0.43-0.67	0.51(0.05)	0.57(0.08)	0.52(0.05)
Brain	0.17(0.04)	0.11-0.24	0.15(0.03)	0.17(0.04)	0.19(0.03)
Breasts	0.22(0.03)	0.17-0.28	0.21(0.03)	0.23(0.04)	0.24(0.03)
Gallbladder wall	0.73(0.11)	0.52-0.94	0.71(0.11)	0.81(0.11)	0.68(0.09)
LLI wall	0.49(0.13)	0.29-0.74	0.51(0.15)	0.49(0.13)	0.48(0.14)
Small intestine	0.36(0.06)	0.26-0.46	0.34(0.06)	0.37(0.07)	0.36(0.05)
Stomach wall	0.35(0.05)	0.27-0.43	0.33(0.04)	0.36(0.06)	0.36(0.04)
ULI wall	0.45(0.08)	0.31-0.58	0.45(0.09)	0.46(0.09)	0.44(0.09)
Heart wall	0.69(0.09)	0.52-0.85	0.63(0.06)	0.70(0.12)	0.74(0.04)
Kidneys	1.36(0.26)	1.02-1.87	1.30(0.23)	1.53(0.29)	1.26(0.18)
Liver	1.67(0.3)	0.99-2.34	1.71(0.24)	1.83(0.32)	1.46(0.24)
Lungs	0.52(0.08)	0.39-0.71	0.53(0.05)	0.52(0.11)	0.50(0.08)
Muscle	0.25(0.04)	0.19-0.33	0.23(0.03)	0.26(0.05)	0.27(0.03)
Pancreas	0.5(0.06)	0.4-0.63	0.47(0.05)	0.52(0.08)	0.50(0.04)
Red marrow	0.32(0.05)	0.23-0.41	0.29(0.04)	0.33(0.07)	0.34(0.04)
Osteogenic cells	0.34(0.07)	0.23-0.46	0.30(0.05)	0.35(0.09)	0.36(0.06)
Skin	0.17(0.03)	0.12-0.23	0.16(0.03)	0.18(0.04)	0.18(0.03)
Spleen	0.76(0.16)	0.49-1.14	0.71(0.10)	0.76(0.25)	0.80(0.08)
Testes	0.19(0.04)	0.13-0.27	0.17(0.04)	0.19(0.05)	0.21(0.04)
Thymus	0.31(0.05)	0.22-0.39	0.28(0.03)	0.31(0.06)	0.33(0.04)
Thyroid	0.21(0.04)	0.15-0.3	0.19(0.04)	0.22(0.05)	0.24(0.04)
Urinary bladder wall	0.25(0.05)	0.18-0.36	0.23(0.04)	0.26(0.06)	0.28(0.04)
Total body	0.3(0.04)	0.23-0.37	0.28(0.04)	0.31(0.05)	0.31(0.04)
Effective dose equivalent (mSv/MBq)	0.54(0.07)	0.43-0.68	0.52(0.05)	0.57(0.09)	0.53(0.04)
Effective dose (mSv/MBq)	0.41(0.06)	0.3-0.51	0.40(0.05)	0.43(0.08)	0.41(0.04)